Heating by optical absorption and the performance of interferometric gravitational-wave detectors

W. Winkler, K. Danzmann, A. Rüdiger, and R. Schilling
Max-Planck-Institut für Quantenoptik, D-8046 Garching bei München, Germany
(Received 6 May 1991)

The ultimate sensitivity of interferometric gravitational-wave detectors requires extremely high light powers sensing the separation of test masses. Absorption of light at the optical components causes wave-front distortions via the thermally deformed substrates or via thermal lensing. The performance of thermally distorted interferometers is treated quantitatively, and the two schemes for increasing the optical path, the delay-line and Fabry-Pérot methods, are compared.

PACS number(s): 04.80.+z, 06.30.Bp, 07.60.Ly, 95.85.Sz

I. INTRODUCTION

The currently planned full scale laser-interferometric antennas for gravitational waves aim at strain sensitivities of 10^{-21} or even 10^{-22} for signals lasting only a few milliseconds [1–3]. It is very likely that events of that strength are produced by astrophysical sources as far out as the Virgo cluster [4, 5]. To achieve the required sensitivity, it is favorable to choose the travel time of the light inside the interferometer to be on the order of the periods of the signals to be observed. An optical path on the order of 100 km will be required for signals in the kilohertz range. For the realization of the long light path one will use an armlength of several kilometers and, in addition, either optical delay lines [6, 7, 1], where each reflection is more or less well separated from the others, or Fabry-Pérot cavities [8, 2], where all the reflections are superimposed, forming one intense beam.

It is the aim of extensive investigations to reduce all relevant noise sources so that the performance is limited only by the shot noise of the detector photocurrent. The highest light power is required for short pulses. To reach a sensitivity of 10^{-21} for millisecond pulses, the interferometer proper will then have to be illuminated with a light power of almost a kilowatt; $\gtrsim 100$ kW are necessary to reach the 10^{-22} level [1]. For longer signal periods and correspondingly increased light paths the power requirements are considerably less. To obtain the high power levels it is planned to use the *recycling* technique, keeping the signal output at a dark fringe and recycling the normally unused light that will be reflected back to the input port of the interferometer [9, 1]. In essence, a resonant optical cavity will be formed that has the locked interferometer as one of its mirrors.

High light power causes severe problems, as there is always some absorption in the optical components. Absorption may take place at the dielectric coatings, and also inside the substrate material in such cases where the beam is transmitted, as in the beam splitter or the coupling mirror of a Fabry-Pérot resonator. The optical components are locally heated and consequently deformed, causing a wave-front deformation of the reflected or transmitted beam.

In addition to the geometric deformation by local heating, a temperature gradient inside the substrate will introduce also a gradient of the index of refraction. This leads to a change in the curvature of the wave front of the transmitted beam, the so-called thermal lensing.

In a delay-line setup there is also a change in the local orientation of the mirror surface at a particular reflection spot because of the tails of the heating at the neighboring spots.

All these effects cannot be expected to cancel out between the two arms, since absorption usually is caused by mechanisms that are not well defined. Because of different conditions in the two arms, the interference quality will not be perfect. In addition, the mode matching between input beam and the modes in the recycling cavity will be deteriorated. Consequently, the possible improvement in sensitivity due to recycling [9] or due to the implementation of squeezed states of light [10–12] (see Sec. VIII) will be limited. This is the reason why a careful analysis of wave-front deformations by local heating is essential for the design and understanding of the performance of interferometers operated at high light power.

Calculations of the effect of thermal lensing and of the substrate deformation by absorbed light power are usually based on numerical solutions of the Navier-Stokes equation; see, for instance, Refs. [13–15]. These elaborate calculations certainly give accurate results for particular input parameters. Nevertheless, for an understanding of the complete interferometer they are impractical because of the large number of parameters to be varied. It is the purpose of this paper to derive simple relations containing all relevant physics. These will allow us to give approximate answers for arbitrary setups without lengthy calculations based on particular parameters. As we will see, our estimates are in good agreement with the elaborate calculations. The simplicity of our approach also allows a variation of a large number of absorption conditions at low computational cost (code and CPU time).

In this paper the considerations are mainly done for the case of delay lines; the problems arising in Fabry-Pérot systems are, however, also treated. First, relations are derived for the relevant mirror deformation caused by

absorbed light power and for the wave-front deformation occurring in a region with a thermally induced gradient in the index of refraction. We then calculate the deterioration of the fringe visibility at the output of the interferometer due to wave-front deformations occurring at the reflection spots inside a delay line. A statistical analysis has been performed on the interference quality and the possible recycling gain was determined as a function of a variety of absorption conditions at the interferometer mirrors. Finally, estimates are given for the sensitivity limits of interferometric gravitational wave detectors.

II. SUBSTRATE DEFORMATION BY ABSORPTION OF LIGHT

A. Heat transport inside the substrate

For a quantitative estimate of the substrate deformation due to absorbed light power, let us first consider the absorption at the dielectric coatings. The heat is removed either by heat conduction or by radiation. For all relevant substrate materials heat conduction is dominant in the immediate vicinity of the reflection spot: The ratio between the power removed by radiation to that removed by heat conduction is given approximately by $4\sigma T^3 w/\kappa$, with σ the radiation constant for the body in question, w the beam radius, κ the thermal conductivity of the substrate material, and T the absolute temperature of the surroundings. Even in the planned large interferometers with several kilometers of armlength, and thus beam radii w_m of the order of 2.5 cm [see Eq. (1)], this ratio is only about 0.1 for fused silica, assuming σ as that of a black body. For other relevant materials like silicon or sapphire the ratio is even smaller because of their higher thermal conductivity and a σ smaller than the blackbody one.

The steepest temperature gradient occurs in the hemisphere inside the substrate with its center at the beam center and its radius equal to the beam radius, see Fig. 1. Outside this hemisphere the heat spreads over a rapidly increasing volume, leading to a weaker temperature gradient there. In equilibrium the entire substrate must radiate all of the power away, since the components are suspended in vacuum for isolation against mechanical noise, and the heat conduction through the thin suspension wire or the surrounding very low pressure gas is several orders of magnitude too small to contribute noticeably.

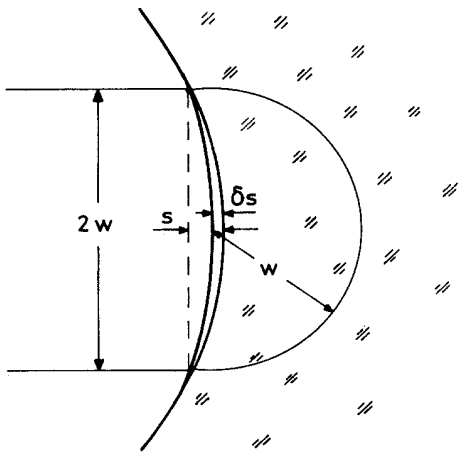

FIG. 1. Absorption of light at the coated surface of optical components is responsible for a temperature gradient across a hemisphere around the reflection spot with radius w. The related thermal expansion of the substrate changes the sagitta s by δs.

At the delay-line mirrors the beam is only reflected and not transmitted. In this case the two most important effects of local heating are, on the one hand, a local change of the radius of curvature of the mirror at the reflection spot in question and, on the other hand, a change in the "average" orientation of the surface at each reflection as caused by the tails of the deformations of the neighboring reflections. Let us first consider the case of wave-front deformations and the corresponding deterioration of the interference quality; the effect of a change in orientation of the beam axis will be treated in Sec. VI.

B. The deformation model

Our model treats the undeformed and the deformed mirror surfaces locally as spherical. The geometrical changes due to absorption-induced expansion are approximated as a change in this local radius of curvature. The rather crude but simple model is justified in retrospect by the good agreement with the elaborate analytical calculations of Hello and Vinet [15]. Their result was 4.3×10^{-8} m of surface deformation across the beam diameter for a mirror with a diameter of 600 mm and a thickness of 200 mm made of fused silica, a beam diameter of 40 mm, and an absorbed light power of 1 W. The results obtained with our simple model deviate from the elaborate analytical calculation by less than a factor of 1.5.

We assume an almost confocal arrangement of the delay lines, and a symmetric mode of the light, i.e., equal beam radii w_m at the far and the near mirrors. The situation in the planned large-scale detectors will not deviate too much from this assumption; generalization to less symmetric cases can easily be made. The beam radius w_m at the mirrors of a delay line (or of a cavity) is in this case given by

$$w_m^2 = \frac{\lambda \ell}{\pi \sin \Theta}, \tag{1}$$

where λ is the wavelength of the light and Θ is defined via the ratio between mirror separation ℓ and radius of curvature R of the mirrors:

$$\cos \Theta = 1 - \frac{\ell}{R}. \tag{2}$$

C. Change in sagitta

The sagitta s, that is the curvature depth of the mirror measured across the beam diameter (see also Fig. 1), is, in the confocal setup, independent of the radius of

curvature: By simple geometrical considerations we get $s \approx w_m^2/(2R)$. For the near-confocal case, R and ℓ are close to each other and $\sin\Theta$ can be replaced by unity. Together with Eq. (1) we get

$$s \approx \frac{\lambda}{2\pi} . \tag{3}$$

This sagitta is the same for cavities or delay lines, and is totally independent of the antenna dimensions, such as the arm length ℓ.

The change δs of the sagitta caused by heating can be estimated by considering the heat transport through the hemisphere around the reflection spot (see Fig. 1) according to

$$P_a = \kappa A \nabla T \approx 2\pi\kappa w_m^2 \frac{\delta T}{w_m} , \tag{4}$$

and the related thermal expansion

$$\delta s \approx \alpha w_m \delta T/2 . \tag{5}$$

Here P_a is the absorbed light power, κ the heat conductivity of the substrate material, A the area through which the heat is transported, α the thermal expansion coefficient, and δT the temperature drop across the hemisphere.

Combining the last two equations we get

$$\delta s \approx \frac{\alpha}{4\pi\kappa} P_a , \tag{6}$$

or, written as a relative deformation,

$$\frac{\delta s}{s} \approx \frac{\alpha}{2\kappa\lambda} P_a . \tag{7}$$

The thermal expansion of the substrate material outside the hemisphere causes a deformation of the mirror surface on a scale much larger than the beam diameter, and thus this bulk effect contributes negligibly to the local curvature change given by Eq. (6). The change in orientation of the mirror surface due to the deformation of the neighboring spots will be treated in Sec. VI.

According to Eq. (7), in the usual case of a positive expansion coefficient, there is a critical absorbed light power of

$$P_{\text{crit}} = \frac{2\kappa\lambda}{\alpha} \tag{8}$$

that would deform the mirror locally, such that its original curvature would be fully compensated; the mirror could then be considered as being flat at this reflection spot. The tolerable deformations are, of course, much less. The crucial quantity for the magnitude of the effect is the ratio α/κ of thermal expansion to heat conductivity. For quantitative estimates it may be useful to list α/κ for a few relevant materials (in units of 10^{-8} m/W): Fused silica 33, sapphire 28, silicon 1.67, ULE ± 2.3 (a material made to have a very low coefficient of thermal expansion), and an astounding but so far purely academic value of 0.13 for diamond. The critical power P_{crit} for fused silica, the most common substrate material, is 3 W. For mechanical reasons, it is not allowed to use Zerodur, another material with a low thermal-expansion coefficient. It has high internal damping, leading to intolerably large thermally excited mechanical vibrations in the relevant frequency range, i.e., below the mechanical resonances of the components [16, 7].

It is important to note that the absolute deformation δs of the curvature depth caused by the absorbed light power does not depend on the beam diameter. In other words, as long as the whole heating process can be described by the linear relations given above for the heat conductivity and the thermal expansion, the relative distortion of the wave front and thus the amount of light shifted into other modes (see below) is independent of the beam size. Thus, it does not help that the area of the reflection spots increases proportionally to the mirror separation.

In practice, one will expect more problems running a small setup at a given light power compared with a large setup, because the higher intensities due to the smaller beam diameter will lead to higher temperatures and temperature gradients. Consequently small setups are more susceptible to irreversible effects, such as damage of the surface layers at a given light power.

D. Magnitude of temperature rise

For a given thermal deformation we can estimate the magnitude of the temperature drop δT across the hemisphere just mentioned by exchanging dependent with independent variables in Eq. (5):

$$\delta T \approx \frac{1}{50\alpha} \left(\frac{\pi\lambda}{\ell}\right)^{1/2} \left(\frac{\delta s}{\lambda/100}\right) . \tag{9}$$

We express the deformation δs in units of $\lambda/100$, a value that [as we will see later; for instance, in Eqs. (18) and (26)] already leads to a significant deterioration of the interference minimum. For a full-scale antenna ($\ell = 3$ km) and for green light ($\lambda \approx 500$ nm, as assumed throughout this paper) the temperature variation across the reflection spot at a deformation of $\lambda/100$ is only on the order of 1 K, taking fused silica as substrate material. In the case of sapphire or silicon we find less than 0.1 K. The average temperature rise of the whole substrate for that particular amount of absorbed light power is also below 1 K. For such small temperature variations, nonlinearities and the stress-induced index errors are expected to be negligible; the linear relations given above can thus be assumed to be valid.

The knowledge of the temperature levels allows one to estimate the time scale of the heating process. It is given by the condition that the absorbed light power has to heat the involved amount of material by the particular temperature difference. For the small hemisphere in question this time scale is on the order of seconds, whereas the heating of the whole substrate may take days to reach equilibrium.

III. THERMAL LENSING

Most materials show a temperature dependence of their index of refraction. Thus, if the light beam is trans-

mitted through a material with a temperature gradient, the heated region of the substrate will act as a lens and thus deform the wave front. This effect is called thermal lensing. The heating may occur because of absorption either in the coating or inside the substrate material.

A. Absorption in the coating

If the absorption takes place at the dielectric coating, the heated region is the hemispherical one already described in Sec. II. For this case a rough estimate of the wave-front deformation of the transmitted beam can be made by considering the effect of a heated hemisphere (as defined above), having a diameter equal to the beam diameter. The difference in light path between the center and the outer parts of the beam is approximately

$$\delta s \approx \beta w_m \delta T/2 \approx \frac{\beta}{4\pi\kappa} P_a . \tag{10}$$

Here δT is the temperature drop across the heated hemisphere, and $\beta = \partial n/\partial T$ the temperature dependence of the index of refraction. These relations are very similar to Eqs. (5) and (6), which describe the change in sagitta caused by thermal expansion. The thermal expansion coefficient α only has to be replaced by β, the temperature coefficient of the index of refraction. Since the argument of Sec. II also applies here, materials with a small ratio of β/κ are required for components through which the light is transmitted in order to get small thermal lensing.

To compare the wave-front distortion due to reflection at a thermally deformed surface with that of transmission through a substrate showing thermal lensing, we only have to compare β and α. For all relevant materials, thermal lensing gives the larger effect. By far the best material in this respect would again be diamond with $\beta/\kappa \approx 10^{-8}$ m/W. Next comes sapphire with 6×10^{-7} m/W. Fused silica is more than a factor of 10 worse than sapphire: 10^{-5} m/W. ULE also has 10^{-5} m/W; it is not as transparent as homogeneous fused silica. Certainly experimental difficulties would arise in the case of sapphire because of its birefringence. On the other hand, its low internal damping (which is expected also for diamond) is desirable in order to keep the thermally excited vibrations small [16, 7].

B. Absorption in the substrate

If the absorption takes place inside the substrate with constant absorption along the light path, we can obtain the temperature distribution in a closed form. The path difference between the beam axis and the e^{-2} point of the light power is described by a relation very similar to Eq. (6):

$$\delta s = 1.3 \frac{\beta}{4\pi\kappa} p_a d . \tag{11}$$

Here p_a is the power absorbed per unit length and d the substrate thickness.

Equation (11) is an example where from a practical point of view it is disadvantageous to choose long arm lengths: The beam diameter grows with the square root of the mirror spacing, and therefore the optical components, such as the beam splitter or the mirrors of a Fabry-Pérot cavity, will have to be bigger as well. The thickness of the components has to be increased correspondingly in order to keep the mechanical resonance frequencies high. Assuming the same absorption level in the substrate for both cases, the larger setup will suffer more from thermal lensing, simply because the length of material traversed will be larger. In addition, the fluctuations in the index of refraction are likely to be bigger on a scale of several centimeters than on a scale of a few millimeters.

The substrate material has to be chosen such that there are no absorption bands in the vicinity of the wavelength used. The absorption is then determined by impurities only. Values in the ppm region (10^{-6} of the incident power) are already critical, as we will see in Sec. V. The internal absorption in a component passed by the light is not well known, particularly at very low absorption levels, since the extinction is mostly dominated by scattering. The few measurements, performed on the purest fused silica samples available, in the visible and in the near infrared show absorption levels on the order of a few ppm per cm [17, 18]. They give an absorption of a few tens of ppm for components with typical dimensions of decimeters in the long-baseline detectors.

IV. WAVE-FRONT DISTORTION AND INTERFERENCE QUALITY

In order to calculate the influence of a wave-front distortion on the quality of the interference, we will, for simplicity, at first assume only one beam to be distorted. The beam parameters at the place of superposition of the two beams, i.e., at the beam splitter, are calculated. In the following we present a few relations that quantify the deterioration of the interference quality; some of them cannot be found in the literature. Since we will assume equal amplitudes for the two beams, the interference minimum is determined by the deviation between the two wave fronts only. Specific attention is given to delay lines. In Sec. V the most important cases of absorption conditions at the optical components are dealt with. The deformations of the mirrors on a scale larger than the beam diameter will be treated in Sec. VI.

A. Equations for ideal delay lines

The beam radius w_n and the radius of curvature R_n of the wave front after the n reflection in a delay line obey the following equations:

$$\left(\frac{w_n}{w_0}\right)^2 = \frac{1}{2}[(1+A) + (1-A)\cos 2n\Theta + B \sin 2n\Theta], \tag{12}$$

$$\frac{R_n}{\ell} = \frac{(1+A) + (1-A)\cos 2n\Theta + B \sin 2n\Theta}{(C-D) + (C+D)\cos 2n\Theta + E \sin 2n\Theta} . \tag{13}$$

The capital letters stand as abbreviations for

$$A = \left(\frac{w_m}{w_0}\right)^4 + \left[\frac{1}{\sin\Theta}\left(\frac{\ell}{R} + \frac{\ell}{R_0}\right)\right]^2 ,$$

$$B = \frac{2}{\sin\Theta}\left(\frac{\ell}{R} + \frac{\ell}{R_0}\right) ,$$

$$C = \frac{\ell}{R_0} ,$$

$$D = \frac{\ell}{R}\left(\frac{w_m}{w_0}\right)^4 + \frac{2\ell}{R\sin^2\Theta}\left(\frac{\ell}{R} + \frac{\ell}{R_0}\right)\left(1 + \frac{\ell}{2R_0}\right) ,$$

$$E = \frac{1}{\sin\Theta}\left[-\frac{2\ell}{R} + \frac{\ell^2}{R_0^2} + \sin^2\Theta\left(\frac{w_m}{w_0}\right)^4\right] .$$

Here w_0 is the radius of the input beam, w_m the radius of the symmetric mode as defined in Eq. (1), R the curvature radius of the mirror at the reflection spot, R_0 the curvature radius of the input wavefront, λ the wavelength of the light, and Θ as defined by Eq. (2). Equation (12) can be found in a paper by Kogelnik [19], and Eq. (13) was derived by using his formalism.

B. Local deformation in delay lines

The effect of a local deformation of a mirror surface on the beam shape was included in the following way. The radius of curvature R_b of the wave front before a reflection is changed to R_a after the reflection according to

$$-\frac{1}{R_a} + \frac{1}{R_b} = \frac{2}{R} , \tag{14}$$

where R is the (possibly distorted) local radius of curvature of the mirror at the reflection spot. The negative sign takes care of the different orientations of R_a and R_b with respect to the direction of beam propagation. The radius of curvature of the deformed wave front R_d after the reflection is related to the value R_u in the undeformed case by

$$\frac{1}{R_d} = \frac{1}{R_u} + \frac{4\,\delta s}{w^2} , \tag{15}$$

where w is the beam radius and δs the change in sagitta, both at the reflection spot in question.

The beam parameters after the reflection are taken as input parameters for Eqs. (12) and (13). If there is only a deformation at the nth reflection, the beam parameters at the output of the delay line can be obtained immediately. In case several or even all of the reflections take place at a deformed surface, one has to proceed stepwise. Eventually the output beam has to be superimposed with the beam from the other arm.

Superposition of two beams gives perfect interference only if the beam parameters are exactly identical. For two Gaussian beams with equal light power but different beam radii w and radii of curvature R, the power at the output of the interferometer reads as

$$\frac{P_{\text{out}}}{P_0} = \frac{1}{2} + \frac{a\sin\phi - b\cos\phi}{w_1 w_2 (a^2 + b^2)} , \tag{16}$$

with ϕ being the phase difference between the two beams, P_0 the total power leaving the interferometer,

$$a = \frac{\pi}{\lambda}\left(\frac{1}{R_2} - \frac{1}{R_1}\right) \text{ and } b = \frac{1}{w_1^2} + \frac{1}{w_2^2} .$$

Solving Eq. (16) for minimum output power with respect to ϕ we get for the relative minimum $p_{\min} = P_{\min}/P_0$:

$$p_{\min} = \frac{1}{2} - \left\{\left[\frac{\pi w_1 w_2}{\lambda}\left(\frac{1}{R_2} - \frac{1}{R_1}\right)\right]^2 + \left(\frac{w_1}{w_2} + \frac{w_2}{w_1}\right)^2\right\}^{-1/2} \tag{17}$$

For the special case of interferometers where the light path is short enough not to change the beam diameter noticeably, we can directly derive a quantitative relation between a particular mirror deformation δs and the resulting deterioration in interference quality. Based on Eqs. (1), (14), (15), and (17) one gets

$$p_{\min} \approx 10^{-3}\left(\frac{\delta s}{\lambda/100}\right)^2 . \tag{18}$$

As we will see in Sec. V, this relation also holds for a long interferometer, and in particular it does not matter at which of the reflection spots inside the delay line the deformation δs occurs.

C. Two ancillary remarks

Equation (18) also helps to specify the tolerable variations δn in the refractive index of a component used in transmission; for instance, the beam splitter. If we assume these variations to occur on a scale d comparable to the beam size, the deteriorated minimum may be as high as

$$p_{\min} \approx 10^{-3}\left(\frac{d\,\delta n}{\lambda/100}\right)^2 . \tag{19}$$

In the most homogeneous fused silica produced so far, fluctuations δn of 2×10^{-7} were found [18]. For that condition and d in the order of a decimeter, the minimum will be deteriorated to about 1%.

Another remark should be made here concerning the wavelength of the light used. For some reasons it seems advantageous to use longer wavelengths than the green argon line at 500 nm; for instance, the fundamental wavelength of the Nd:YAG (where YAG denotes yttrium aluminum garnet) laser at 1000 nm. It is this laser, in particular the diode pumped version, that promises to combine high light power with high efficiency.

As the shot-noise-limited sensitivity depends on the ratio between wavelength and light power, an increase in wavelength has to be accompanied by a corresponding increase in power to get the same performance [see, for instance, Eq. (34)]. On the other hand, a deformation δs is proportional to the absorbed light power. For a wavelength-independent absorption the deterioration

of the interference quality would then remain the same; see, for instance, Eqs. (18), (19), and the relations in the following sections. From this point of view there would be no difference in using shorter or longer wavelengths. But usually absorption and scattering are lower at longer wavelengths. One drawback for that case—more severe for delay lines than for cavities—is the larger mirror diameter required.

D. Mismatch between beam and Fabry-Pérot cavity

Local heating changes either the wave front of the passing beam or the shape of the eigenmodes inside a Fabry-Pérot resonator. In the following we give a collection of useful formulas for an estimate of the related coupling loss between the incoming beam and the eigenmodes of the cavity.

From the relations for the beam radii of the fundamental mode at the cavity mirrors, given by Kogelnik [19], we get

$$w_1^2 = \frac{\lambda \ell}{\pi} \left(\frac{g_2}{g_1(1-g_1 g_2)} \right)^{1/2}, \tag{20}$$

$$w_2^2 = \frac{\lambda \ell}{\pi} \left(\frac{g_1}{g_2(1-g_1 g_2)} \right)^{1/2}, \tag{21}$$

with $g_1 = 1 - \ell/R_1$ and $g_2 = 1 - \ell/R_2$. In order to determine the coupling of the input mode to the cavity eigenmode, we need the parameters of the eigenmode at the coupling mirror. The radius of curvature of the mode equals the local radius of curvature of the mirror, even when this mirror is locally deformed. The mode radius at the coupling mirror depends on the shape of both mirrors, as described by Eq. (20). The dependence of the mode radius at the coupling mirror on a deformation either of the near or of the far mirror is given by the following relations: Local heating may change the sagitta by δs_1 at the coupling mirror (and thus also of the mode there) and by δs_2 at the far mirror. The respective changes in mode radius at the coupling mirror are given by

$$\frac{\delta w_1}{w_1} = \frac{\pi}{2\lambda} \frac{1 - 2g_1 g_2}{[g_1 g_2 (1 - g_1 g_2)]^{1/2}} \delta s_1 , \tag{22}$$

and

$$\frac{\delta w_1}{w_1} = -\frac{\pi}{2\lambda} \frac{1}{[g_1 g_2 (1 - g_1 g_2)]^{1/2}} \delta s_2 . \tag{23}$$

Let us call δs the difference in sagitta between the wave front of the incoming beam and the mode at the coupling mirror. The fraction of light that is not coupled into the cavity, but rather reflected, is

$$\frac{\delta P}{P} \approx \left(\frac{\pi \delta s}{\lambda} \right)^2 . \tag{24}$$

A similar expression holds for a mismatch in beam radius:

$$\frac{\delta P}{P} \approx \left(\frac{\delta w}{w} \right)^2 . \tag{25}$$

V. NUMERICAL DETERMINATION OF CRITICAL ABSORPTION LEVELS

This section summarizes the results of a computer simulation of the interferometer performance for relevant absorption levels at the interferometer components, particularly at the delay-line mirrors. The calculations were based on the formulas given in the previous sections. In this context one should again mention how the heating effects scale with the armlength of an interferometer. As already stated in Sec. II.C, there is no difference between a small and a large setup in the deterioration of the interference quality for a given amount of absorbed light power, as long as the physical effects are linear. This statement was verified by our computer simulations.

The subsequent examples are in some sense arranged for growing complexity. Starting from an ideal interferometer, at first, absorption at only one reflection spot is assumed. Next follows uniform absorption at all reflections of all mirrors, then uniform absorption across the surface of one mirror and all other components without losses; one example describes the case of constant absorption across the surface of each mirror, but one mirror is different. Finally the absorption is varied statistically from one reflection spot to the next.

A. Deformation at one of the reflection spots inside a delay line

For a quantitative estimate of the effect of a particular deformation it is useful to consider first a deviation from ideal conditions at only one out of the many reflections. The parameters of the beam reflected at a deformed part of the mirror surface are determined, used as the input parameters for Eqs. (12) and (13), and eventually the beam parameters at the output of the interferometer are calculated. These will differ from those of the undistorted beam, and therefore the interference quality will be deteriorated.

Whether the mismatch in beam diameter or in curvature of the wave front dominates depends on the location of the reflection along the beam path where the deformation took place. But the fringe contrast does not: A given mirror deformation δs (as defined earlier) at any of the reflections in a delay line leads to the same deterioration of the interference minimum. This is consistent with the notion that a reflection at a particular mirror deformation shifts a certain amount of light out of the given light mode into other modes that do not interfere with the original one.

In agreement with Eq. (18), valid for a short interferometer, the results of numerical calculations for different deformations δs in a long interferometer can be summarized as

$$p_{\min} \approx 10^{-3} \left(\frac{\delta s}{\lambda/100} \right)^2 , \tag{26}$$

no matter at which reflection the deformation occurred. This means that introducing a mirror deformation δs of $\lambda/100$ at *any* of the reflection spots in an interferometer

with otherwise perfect delay-line mirrors gives a relative minimum at the output of 10^{-3}, corresponding to a visibility V of 0.998; the visibility is defined in the usual way as $V = (p_{\max} - p_{\min})/(p_{\max} + p_{\min})$. The magnitude of the relative minimum is proportional to the square of the change in sagitta. It is the absolute value of δs that counts, and not, as one might expect, the relative distortion $\delta s/s$. This is so because the path difference between the center and the outer parts of the beam is responsible for the deterioration in interference quality. In other words, if the beam inside the delay line is reflected at a dip (or a bump), with the same diameter as the beam, then the deterioration of the interference quality is the same whether beam and dip have a big or a small diameter, provided the absolute deviation δs of the curvature depth relative to the undisturbed case is the same.

B. Uniform absorption at all mirrors

In general there will be some absorption at *each* of the reflections. The corresponding distortions δs do not add up linearly for the successive reflections; rather a sinusoidal variation of the beam parameters is introduced, as one can see from the following consideration. Let us, for simplicity, assume the matched case (where all reflection spots initially have the same diameter) and a constant absorption. Corresponding to a given change in sagitta δs there will be a change of the local radius of curvature of the mirrors. Its value determines the parameters of the wave front at the subsequent reflections and at the output of the delay line, as defined in Eqs. (12) and (13). As far as the shape of the wave front is concerned, the deformed delay line can therefore be described by the new local radius of curvature and the corresponding Θ value.

As long as the absorption is constant and equal for all of the delay-line mirrors, the interferometer remains symmetric and the interference at the beam splitter will be perfect, unless other limitations such as an unpracticably large beam size occur. But there will be a degradation for the recycling schemes: Since the mirror separation was chosen to fulfil the reentrance condition in the delay line (that is, a reproduction of all the beam parameters of the input beam by the output beam) for the original radius of curvature, with the new local radius of curvature the reentrance condition in general will be violated with respect to the shape of the wave front. The input and output beams will therefore differ in shape, leading to an imperfect-mode match between the entering light beam and the modes in the recycling cavity (see Secs. IV A and IV D). This mismatch can be partly compensated for by readjusting the mode that impinges on the recycling mirror.

C. Uniform absorption at one mirror

A more realistic experimental situation may be the case where the absorption across each individual mirror surface is still constant, but where one of the mirrors absorbs significantly more than the other ones. The behavior of this one mirror then dominates the interference quality.

Let δs be the mirror deformation at each of the reflections at this particular mirror. In Fig. 2 the relative interference minimum of an interferometer containing such a mirror is plotted against the local mirror deformation δs, which in turn is proportional to the absorbed light power. Figure 2(a) describes the subconfocal case ($\ell < R$) and 2(b) the superconfocal one ($\ell > R$). For all plots in this section, $N = 34$ beams in each delay line and green light were assumed.

Increasing the light power from very small values, the interference quality deteriorates in a nonlinear fashion. Most striking is the different behavior of the sub- and the superconfocal arrangements. In case of a mirror spacing larger than confocal, the interference quality deteriorates monotonically [Fig. 2(b)], whereas in the subconfocal case the interference quality improves again after a peak deterioration of the minimum to about 10% [Fig. 2(a)]. A plot of the beam shape after each reflection, as well as numerical calculations, showed that for particular values of δs, the output beam may again have the same shape as in the undistorted case $\delta s = 0$, in spite of the large oscillations of the beam parameters inside the delay line; this is consistent with the plot in Fig. 2(a).

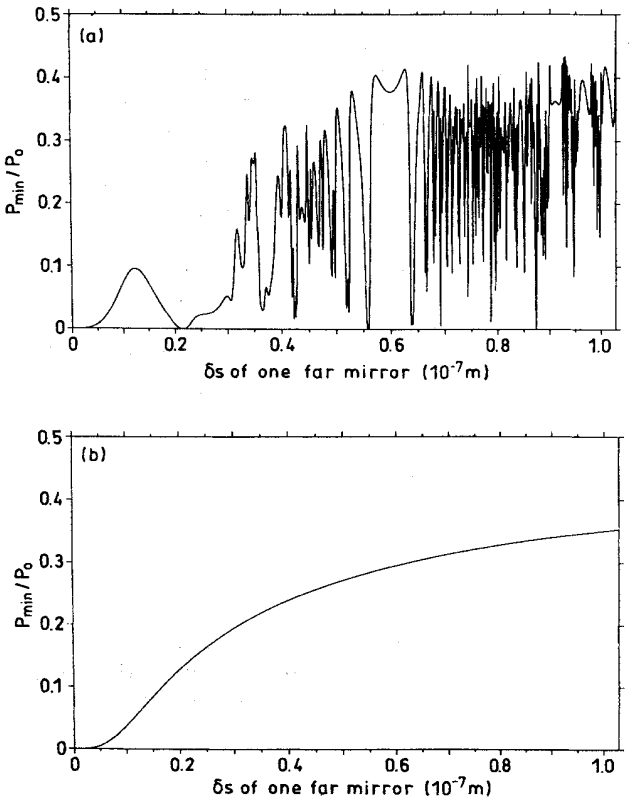

FIG. 2. Interference minimum of a Michelson interferometer with delay lines and containing one absorbing mirror, as a function of the local mirror deformation δs, which is proportional to the absorbed light power: (a) for mirror spacing smaller than the confocal distance (subconfocal); (b) for mirror spacing larger than confocal (superconfocal).

It is beyond the scope of this paper to comment on the transition from a smooth to a chaotic looking behavior of the interference quality with growing deformation in the subconfocal configuration. For our purpose we want to stay in the region of good interference, i.e., below the first maximum in Fig. 2(a). That part of the curve can be approximated by the relation

$$p_{\min} \approx 10^{-3} \left(\frac{N\,\delta s}{\lambda/5} \right)^4 . \tag{27}$$

A numerical example for illustration: For 34 reflections a deformation of as little as $\lambda/200$ at each of the reflections at one mirror already leads to an interference minimum of 10^{-3}, and $\lambda/100$ gives more than 10^{-2}.

D. One mirror having stronger absorption

Next we treat the case where the absorption is constant across the surfaces of each of the four delay-line mirrors, but higher at one of them by a factor f. Figures 3(a) and 3(b), respectively, show the subconfocal and the superconfocal cases for $f = 1.5$.

Here δs is the deformation of the three identical mirrors, whereas the fourth mirror has a deformation of $f\,\delta s$. The relevant part in Fig. 3(a), below the first maximum, can be described by

$$p_{\min} \approx 2 \times 10^{-3}\,(f-1) \left(\frac{N}{34} \frac{f\,\delta s}{\lambda/100} \right)^{3.5} \tag{28}$$

A comparison between Figs. 3(a) and 3(b) gives an example of the superiority of the subconfocal setup ($\ell < R$) over the superconfocal one: The first peak in Fig. 3(a) only has a height of about 1%, whereas this peak exceeds 10% in the other case. The difference is particularly striking for the more symmetric case of $f = 1.2$ shown in Figs. 3(c) and 3(d).

For very small asymmetry of the mirrors, say f somewhere between 1 and 1.1, the first peak of the subconfocal setup stays below 10^{-3}, and the power is allowed to increase until the second peak becomes relevant. The behavior of the superconfocal setup can be made plausible by considering the well-known stability diagram for Fabry-Pérot cavities; see, for instance, Ref. [20]. For given radii of curvature of the mirrors it shows the mirror spacings where stable eigenmodes can be established. If one applies these stability criteria to the local curvature of the mirrors, one can easily see that in the superconfocal case a relatively small deformation $\delta s = \lambda/(2N)$ is sufficient to bring the setup to the boundary of the stable region. Fairly small fluctuations in surface deformation

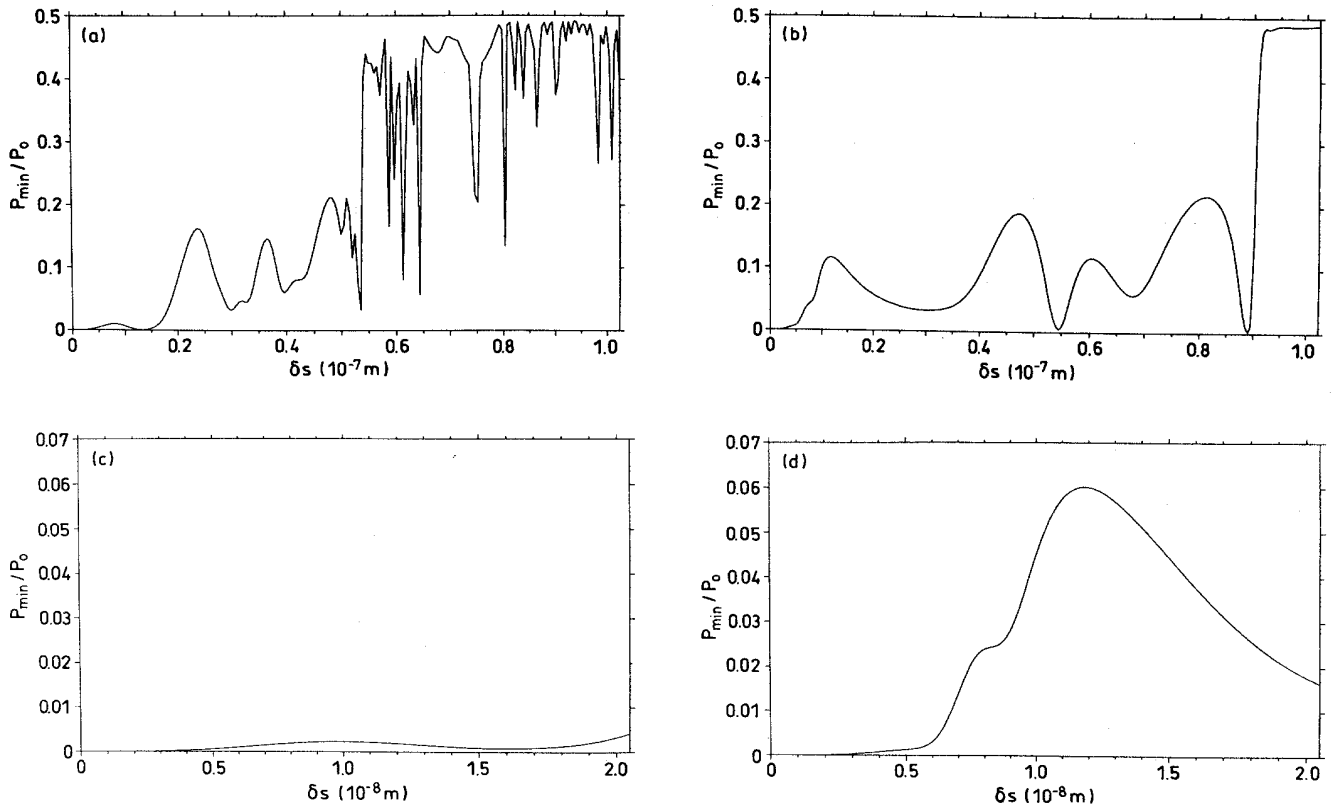

FIG. 3. Interference minimum of a Michelson interferometer with delay lines containing mirrors with constant absorption. (a) One mirror absorbs 50% more than the other ones, subconfocal mirror spacing; (b) same as (a), but superconfocal mirror spacing; (c) one mirror absorbs 20% more than the other ones, subconfocal mirror spacing; (d) same as (c), but superconfocal mirror spacing.

then lead to relatively large fluctuations in beam shape, thus deteriorating the interference quality more than in the case of the subconfocal arrangement.

E. Statistically fluctuating absorption levels at successive reflection spots

In a real interferometer one does not expect the absorption to be constant across the whole surface of the mirrors, but rather to exhibit some fluctuation. We now consider a situation where all four delay-line mirrors show the same *average* absorption, leading to an average deformation Δs. In addition, we assume a statistical fluctuation of δs as described by its standard deviation s_d. Averaged over many such interferometers with subconfocal mirror spacing we find a deteriorated interference minimum of

$$p_{\min} \approx 5 \times 10^{-2} \frac{N}{34} \left[\left(\frac{s_d}{\lambda/100} \right)^2 + 0.15 \frac{N}{34} \left(\frac{s_d}{\lambda/100} \right)^{3/2} \frac{\Delta s}{\lambda/100} \right]. \tag{29}$$

An example for the subconfocal and the superconfocal cases is shown in Figs. 4(a) and 4(b). The sudden increase that can be seen for the superconfocal delay line is related to the strong peak in Figs. 3(b) and 3(d), and is certainly not desirable.

F. Statistically fluctuating absorption levels and stronger absorption at one mirror

Finally, for completeness, the case should be treated where three of the mirrors show the same average absorption, corresponding to an average deformation Δs and equal fluctuation as described by the standard deviation s_d, whereas the fourth mirror shows a mean deformation $\Delta s_1 = f \Delta s$ and a standard deviation of $s_{d1} = f s_d$. This case is not really new; it is covered by Eq. (29). For f very close to 1 the relation remains unchanged; for $f > 1.2$ the more strongly absorbing mirror dominates and its values for Δs and s_d have to be inserted in Eq. (29). Of course, the fact has to be taken into account that now only one mirror is involved with fewer reflection spots than all four.

G. Wave-front deformation and the number N of reflection spots

We also investigated the deterioration of the interference quality as a function of the number of reflections at an imperfect surface. If the surface deformation fluctuates statistically from one reflection to the next, numerical simulations show that the wave-front deformation on average grows with the square root of the number N of reflections, whereas the interference minimum deteriorates proportional to N. This result can also be obtained from Eq. (29) for $\Delta s \to 0$. The relation then reduces to

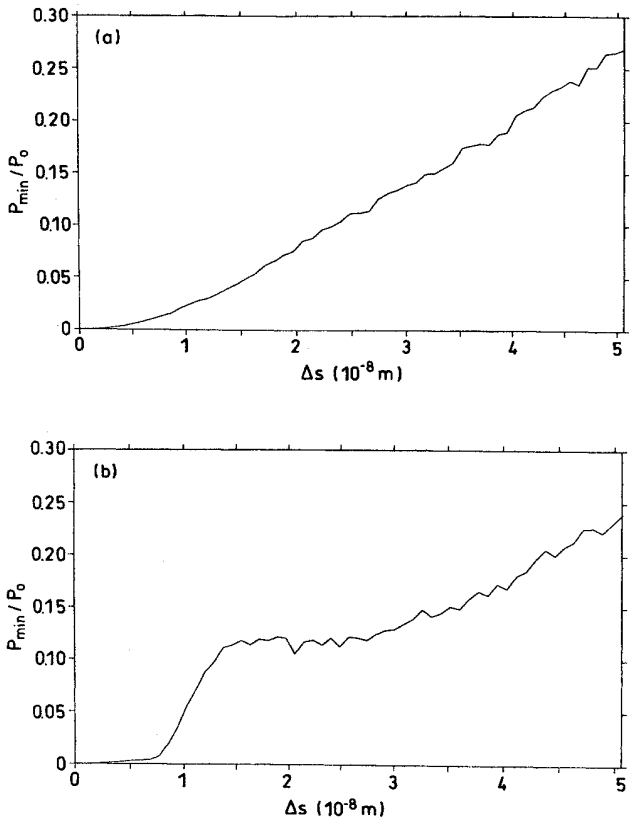

FIG. 4. Interference minimum of a Michelson interferometer with delay lines, containing mirrors with an absorption fluctuating statistically from one reflection to the next. In addition to an average deformation Δs a statistical fluctuation with a standard deviation of $s_d = 0.25 \Delta s$ was assumed and the ensemble average over 1000 such interferometers was plotted: (a) for subconfocal mirror spacing; (b) for superconfocal mirror spacing.

$$p_{\min} \approx 5 \times 10^{-2} \frac{N}{34} \left(\frac{s_d}{\lambda/100} \right)^2. \tag{30}$$

This means that the interference minimum is degraded to about 5% for an interferometer with delay lines and 34 bounces in each arm, with surface deformations extending over lateral dimensions in the order of the beam diameter, fluctuating statistically with a standard deviation of $\lambda/100$.

This result has consequences concerning the manufacturing of large mirrors. As is well known, the spectrum of the surface irregularities of a mirror produced by today's state of the art shows a strong increase towards longer spatial wavelengths. In a long-baseline setup the beam diameter is large; this means that the related wave-front deformation and thus the interference quality will be worse than in a short one, allowing less power buildup by recycling. The requirement for the surface figure of the mirrors at spatial wavelengths on the order of the beam diameter can be obtained using Eq. (30). It may be planned, for instance, to implement power recycling in

an interferometer with delay lines supporting 34 beams each. If deviations of the mirror surface with respect to an ideal sphere on a scale in the order of the beam diameter stay below $\lambda/500$, we find an interference minimum of 2×10^{-3}, permitting a recycling power buildup of a few hundred. The deformations with periods shorter than the beam diameter, usually called microroughness, give rise to scattering losses. These may also limit the recycling power buildup. In order to allow an enhancement of a few hundred, the corresponding amplitudes have to be even smaller than $\lambda/500$.

VI. LOCAL HEATING AND BEAM POSITION

In the preceding sections we considered the spherical deformation of the wave front caused by substrates that are locally heated by the beam itself. Besides this axisymmetric distortion, the expansion due to local heating also changes the orientation of the mirror surface at the neighboring reflections in a delay line because of the tails of the temperature distribution around a heated spot. These tails primarily have two effects. First they lead to a displacement of the output beam, which can easily be compensated for if multimirror delay lines are used instead of the usual two-mirror delay lines [7, 1]. Second, these large-scale deformations of the mirror surface also distort the beam shape, just as astigmatic mirrors do [see Eqs. (2), (12), and (13)]. The latter effect is negligible in our case as long as the beam is not focused too strongly. In the case of the long baselines one will avoid strong focusing anyhow because of the larger mirror sizes required.

A. Beam displacement

Let us now estimate the magnitude of the beam displacement due to the tails of the heating at the different reflection spots. The average orientation of the mirror surface at each spot center is responsible for the direction of propagation of the beam axis after that reflection. To define the orientation of the surface it is sufficient to know the slopes in the radial and in the tangential directions. Because of symmetry, the orientation in the tangential direction is not changed if the two neighboring spots are heated in the same way. But in the radial direction the center of the spot is further out than the interconnection between its neighbors. There the tails of the neighboring bumps are on the decline and thus a larger global radius of curvature is simulated. As a consequence, the reentrance condition is violated for the beam position: The output beam of the delay line is shifted relative to the input beam by δy, tangentially to the circle of the reflection spots.

This displacement δy can be calculated from a given variation δR of the radius of curvature R of the mirror (as defined by the surface orientation) by

$$\delta y = \frac{N w_c \ell \, \delta R}{R^2 \sin \Theta} . \tag{31}$$

Here w_c is the radius of the circle of the reflection spots, again N is the number of beams, ℓ is the mirror separation, and Θ is defined in Eq. (2). In the near-confocal case Eq. (31) can be approximated by

$$\delta y \approx N w_c \frac{\delta R}{R} . \tag{32}$$

If the heating were exactly the same in the two (symmetric) arms, each of the two beams running back to the beam splitter would be shifted in the same way, still yielding a good interference quality. But there are other consequences, even in case of a symmetric heating. For instance, a shift or a bending of the wave front of the output beam that is used for recycling would degrade the mode match to the input beam, and consequently limit the power buildup inside the interferometer. In addition, as already stated, a certain asymmetry between the two arms has to be expected, leading to a relative displacement between the interfering beams. Such a relative displacement δy gives, for otherwise perfect conditions, a relative power in the interference minimum of

$$p_{\min} = \frac{1}{2}\left\{1 - \exp\left[-\frac{1}{2}\left(\frac{\delta y}{w}\right)^2\right]\right\} \approx \left(\frac{\delta y}{2w}\right)^2 , \tag{33}$$

where w is the beam radius.

These equations allow an estimate of the deterioration of the interference quality due to a relative displacement between the two interfering beams produced by asymmetric heating in the two arms. Based on the values for the deformation given by Hello and Vinet [15], the deterioration due to the relative beam displacement is less than that produced by the change in radius of curvature of the wave fronts, assuming a separation of two or three beam diameters between the centers of neighboring reflection spots.

B. Restoring the reentrance condition

The reentrance condition for the beam position could in principle be restored by adjusting the mirror separation relative to the new effective radius of curvature. But the distance over which the mirrors would have to be shifted is impracticably large, even for slight deformations. Another possibility is the use of multimirror delay lines in the arms of the interferometer. In this case, orientation and position of the output beam are defined by the orientation of the mirrors. A simple example is a standard delay line with two coupling holes in the near mirror: The beam enters through one hole and after several reflections leaves through the other one. Here it hits a return mirror perpendicularly and retraces its original path. Position and orientation of the output beam can now be controlled via the orientation of the return mirror [1].

The arrangement with a retromirror is particularly useful for the implementation of the recycling schemes. The bright fringe output beam of the interferometer retraces the input beam, and therefore it is sufficient to insert one properly chosen mirror between the laser and the interferometer to install power recycling. A similar ar-

gument holds for signal recycling at the measurement output port. Thus, the multimirror delay line helps to solve the problem of a relative displacement between the two interfering beams; but there is no simple solution to the more severe change in curvature of the wave front due to local heating.

VII. POWER RECYCLING AND WAVE-FRONT DEFORMATION

In a perfect interferometer the single-sided spectral density of the shot-noise-simulated fluctuations in path difference δL is given by [21]

$$S_{\delta L}(f) = \frac{\hbar c}{\pi} \frac{\lambda}{\eta P_{\text{circ}}}. \tag{34}$$

Here $\hbar$ is Planck's constant $h/2\pi$, c is the speed of light, λ the wavelength of the light, η the quantum efficiency of the photo diode, and P_{circ} the effective light power inside the interferometer; for instance, the power running back to the beam splitter. (In this sense the multiple reflection scheme used in the arms of the interferometer, either delay line or Fabry-Pérot cavity, does not increase the usable light power P_{circ}—it only matches the storage time of the light to the period of the signal to be observed.)

For the detection of millisecond pulses of gravitational radiation at a strain level of 10^{-21}, it is necessary to have an effective light power P_{circ}, as just defined, of about 1000 W (see, for instance, Refs. [1], [4], and [22]). For signals with longer periods the optical pathlength may be increased and the bandwidth of observation may be reduced, allowing to arrive at the same strain sensitivity with less light power. But the effective light power is in any case a good measure for the potential sensitivity of a large-scale interferometer that has been optimized in other respects. Implementation of power recycling is a useful means to increase the amount of light sensing the positions of the mirrors. In the case of an imperfect interference the power P_{min} of light leaves the interferometer through the measurement output port; it has to be counted as a loss and thus reduces the possible gain in sensitivity by power recycling.

In order to extract the signal from the interferometer output at the dark fringe it is necessary to use some modulation technique; see, for instance, Ref. [23]. One can either phase modulate the interfering beams relative to each other (internal modulation), or superimpose the interferometer output beam with a modulated reference beam (external modulation). To achieve a maximum signal-to-noise ratio, both modulation techniques require the relative amount of light that on average leaves the interferometer to be noticeably increased above the minimum output power. This extra loss can be kept small if the output beam is sent through a mode cleaner with low losses; in this case only light in the fundamental mode of the radiation field will reach the photodiode. This measure improves the effective interference contrast and therefore allows a smaller modulation amplitude for internal modulation and a weaker reference beam for external modulation. For the following calculations we have assumed a mode cleaner at the output of the interferometer, leaving only the losses due to the imperfect fringe contrast. In this picture the aberrations just shift light out of the original fundamental mode of the radiation field into orthogonal higher-order modes and there is no additional degradation of the interference quality.

A. Power enhancement with present technology

The limitation that the performance of Michelson interferometers suffer by local heating will be demonstrated in Figs. 5–7. They were obtained by including scattering and absorption at the optical components in otherwise perfect interferometers and calculating the degradation of the interference because of thermal lensing and thermal expansion as a consequence of local heating. In some sense, we have used a worst-case scenario: The amplitudes of all wave-front deformations add in the same direction, and thermal lensing is compensated only when indicated in the text.

As a measure of the degradation, the required input power P_{in} is plotted against the effective light power P_{circ} that builds up inside the interferometer under the condition of correspondingly deformed wave-fronts. Some relevant substrate materials and several levels of absorption and unbalance in absorption have been chosen. In Figs. 5 and 6, scattering and absorption at the optical

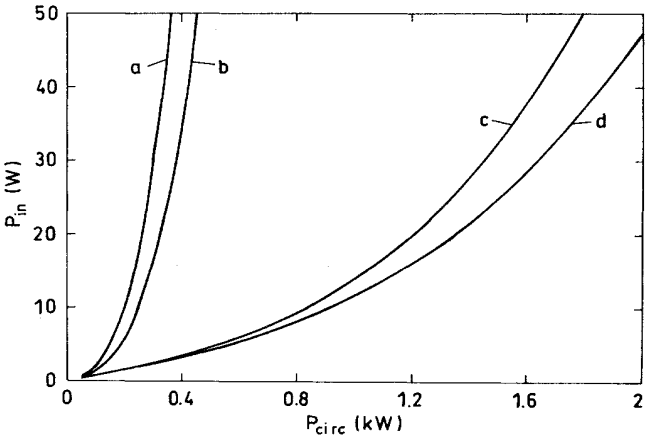

FIG. 5. Power recycling with thermal distortion. The required input power P_{in} for an interferometer with a Fabry-Pérot cavity in each arm is plotted against the circulating light power P_{circ} appearing for instance at the recycling mirror. A complete interferometer was simulated, including losses by scattering, absorption, and wave-front distortion by thermal lensing and thermal expansion of locally heated substrates. Rayleigh scattering of 200 ppm in each component passed by the laser beam was assumed, substrate absorption of 20 ppm, coating loss of 50 ppm, coating absorption of 20 ppm, transmission of the coupling mirror equivalent to a light path of 34 beams, unbalance in coating absorption of 20%, and unbalance in substrate absorption of 10%. (a) Setup made of fused silica; (b) same as (a), but thermal lens in the beam splitter compensated by the compensation plate down to 10%; (c) all components made of sapphire; (d) same as (c), but compensation as in (b).

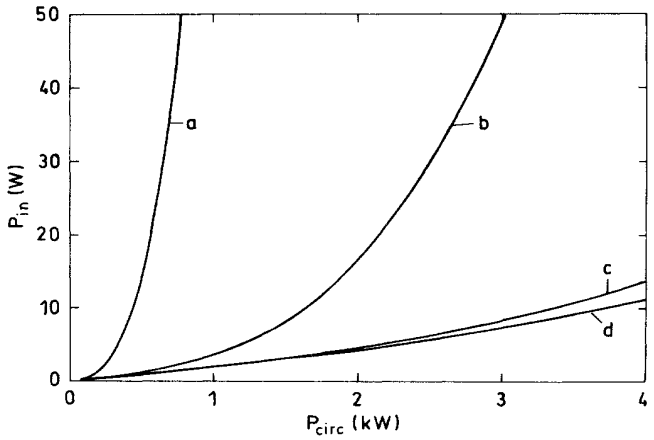

FIG. 6. Same as in Fig. 5, but for delay lines; on top of an average mirror deformation Δs a statistical fluctuation with a standard deviation $s_d = 0.2\Delta s$ was assumed: (a) a fused silica setup, no compensation of thermal lensing. For (b), (c), and (d) compensation of the beam-splitter lens as in Fig. 5 (b) was assumed: (b) a fused silica setup; (c) sapphire beam splitter and fused silica mirrors; (d) sapphire beam splitter and silicon mirrors.

components were assumed to be as low as that which seems realistic with today's state of the art for green light; Fig. 7 gives the results for optimistic assumptions that may be realized with future technology.

The numbers used in Figs. 5–7 should be compared with the numbers that are valid for components manufactured corresponding to today's state of the art: The lowest losses in coatings reported so far for visible light

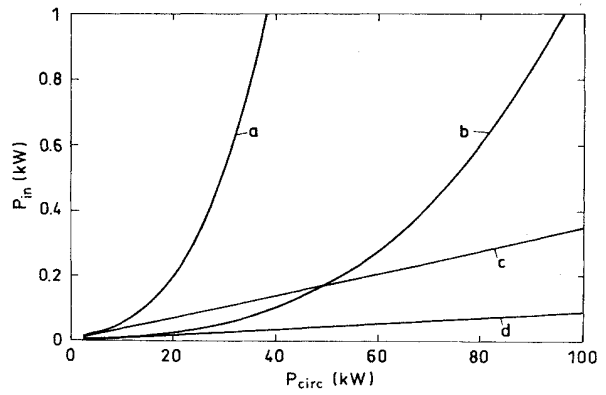

FIG. 7. The same as in Figs. 5 and 6, but with optimistic assumptions. Rayleigh scattering again 200 ppm per traversed component, substrate absorption 10 ppm, coating loss 20 ppm, coating absorption 2 ppm, 34 beams in each arm, and an unbalance in absorption (coating and substrate) of 10%. Thermal lens in the beam splitter compensated to 10%: (a) a cavity system made of sapphire; (b) a delay-line system with a sapphire beam splitter and silicon mirrors; (c) Fabry-Pérot setup made of diamond; (d) delay-line setup made of diamond.

have been some 10 ppm per reflection. Recently we have measured 25 ppm total loss and 2 ppm absorption for green light, at coatings produced with an ion sputtering technique. As an example, for materials with low internal absorption one may take, as already mentioned in Sec. III B, the purest fused silica samples available today. They show absorption levels on the order of a few ppm per centimeter, equivalent to a few tens of ppm for the typical thicknesses of the components in the long-baseline detectors.

For Figs. 5–7 the coating absorption was described by an average value and a statistical fluctuation; see Eq. (29) for delay lines, and Sec. IV D for cavities. So far, values for the standard deviation s_d are not well known; $s_d/\Delta s = 0.2$ seems to be rather on the optimistic side.

Figure 5 describes a Fabry-Pérot configuration. Curve *a* shows the worst performance of our examples. It was obtained for a setup made of fused silica. Most striking is the steep nonlinear increase in required input power if the usable light power P_{circ} is to be raised. The most severe restriction is due to thermal lensing in the coupling mirrors of the Fabry-Pérot cavities. This effect is a consequence of absorption of light inside the traversed substrate material and of absorption at the surface coating. The latter contribution is the more critical as it is related to the reflection of enhanced power *inside* a cavity. But absorption in the substrate is also significant. The contribution of thermal lensing in the beam splitter is of minor importance, as a 90% compensation of this effect only gives the improvement from curve *a* to curve *b*. The thermal lens in the coupling mirror of the Fabry-Pérot cavities is reduced by the use of sapphire substrates, see curve *c*. The effect of the thermal lens in the beam splitter is still of minor importance, as its compensation only gives the small change from curve *c* to *d*.

Somewhat better performance is obtained for a delay-line system also made of fused silica; see curve *a* in Fig. 6. Here the dominating effect is thermal lensing in the beam splitter; this thermal lens may also stand for a mismatch in thermal lensing between beam splitter and compensation plate. A 90% compensation of the lensing effect improves the performance from curve *a* to curve *b*. The best performance of the examples shown in Figs. 5 and 6, i.e., curve *d* in Fig. 6, results from a combination of the optimum choices (as long as diamond is not available): a delay line scheme (yielding lower light intensity at the reflection spots for a given P_{circ}), silicon mirrors (for low α/κ, possible only for delay lines), and a sapphire beam splitter (best transparent material).

B. Power enhancement with future technology

Figures 5 and 6 show very impressively the effect of local heating in a high-power interferometer. Obviously it will be rather difficult to realize several kilowatts of effective light power inside the interferometer, as long as fused silica is used as the substrate material for the relevant optical components, even for the case of optical delay lines. It is particularly the strong thermal lensing of fused silica that limits the performance.

For higher light power it is mandatory to choose materials with better thermal properties. Thermal problems arising in a setup planned for the 10^{-22} strain level at an observational frequency of 1 kHz may be overcome with the parameters chosen for Fig. 7. The effective power level to be aimed at is about a 100 kW. The substrate materials are rather unusual from today's point of view, and the losses are assumed to be very small: substrate absorption of 10 ppm, coating loss of 20 ppm, coating absorption of 2 ppm, and an asymmetry in absorption between the two arms of 10%, i.e., $f = 1.1$. From these plots one can conclude that the 100-kW level is not out of reach, but certainly much more difficult to realize with Fabry-Pérot than with delay-line interferometers.

The plots also show that diamond would be an ideal substrate material. Thermal effects lead to a nonlinear relation between P_{in} and P_{circ}, and thus the linear curves c and d for diamond indicate that for the low absorption assumed in the plot, the thermal effects are negligible and the losses—even at such high power levels—are totally dominated by scattering.

Figures 5–7 have been obtained assuming perfect interference at low light power. In a real setup there will be a finite visibility because of nonideal components. Let us consider as a practical example the wave-front deformation caused by a real beam splitter. As already mentioned in Sec. IV, the most homogeneous fused silica produced so far shows fluctuations in the index of refraction on a scale of decimeters of about 2×10^{-7}. For a beam diameter and a traversed length both comparable to a decimeter, the sagitta of the beam would be changed by $\lambda/25$. According to Eq. (26) the corresponding relative interference minimum would be about 1%, limiting the power enhancement $P_{\text{circ}}/P_{\text{in}}$ to a factor on the order of 100. The same wave-front deformation, but caused by the temperature dependence of the index of refraction, would result from an absorption of 25 mW in that component.

As already stated above, the plots are based on a 3-km setup optimized for millisecond pulses. Lower observational frequencies would allow us to realize the same strain sensitivity with less light power.

VIII. SQUEEZED STATES AND WAVE-FRONT DEFORMATIONS

Obviously an elegant solution to the heating problem would be the use of squeezed states of light in order to lower the shot-noise level instead of using higher light powers. In this section we will investigate what gains are obtainable with this alternative.

The idea of noise reduction beyond the level set by the Poisson statistics was developed by Caves [10]. The statistical fluctuations in the number of photons detected at the photodiode are described as a consequence of the vacuum fluctuations of the electromagnetic field at the second, normally unused, input port of the interferometer. It turns out that in an otherwise perfect interferometer the fluctuations in the phase of this field determine the statistics of the number of photons in the output beam, the well-known shot-noise limit. This noise can be reduced by sending light into the second input port with phase fluctuations less than those of the vacuum state. The existence of these so-called squeezed states of light has already been shown experimentally; see, for instance, Ref. [24]. Unfortunately, squeezed states are very fragile. Already in his first paper Caves pointed out the influence of losses; for instance, reflection losses at the optical components or imperfect quantum efficiency of the photodiode. Indeed, the possible gain in sensitivity by use of squeezed states is at least as severely limited by an imperfect interference as the power recycling scheme.

The relations relevant to the case of nonideal conditions, particularly of imperfect interference, have been developed by Gea-Banacloche and Leuchs [12]. The fluctuations in phase difference simulated by the Poisson statistics at the output of a perfect interferometer are given by

$$\delta\phi_{\min} = 1/\sqrt{n}\,. \tag{35}$$

Here n is the number of photons sensing the position of the mirrors within the chosen resolution time. For an ideal interferometer the gain in sensitivity due to the application of squeezed light is proportional to the amount of squeezing, $1 - e^{-s}$. In this picture $s = 0$ means no squeezing. An imperfect visibility V limits the possible improvement to

$$\delta\phi_{\min} = \left(\frac{[2(1-V)]^{1/2} + e^{-2s}}{n}\right)^{1/2}. \tag{36}$$

Thus, even for an arbitrarily high degree of squeezing the gain in sensitivity is limited to $[2(1-V)]^{1/4}$. This means that an interference minimum of 10^{-4}, which seems very optimistic, would allow a factor of 7 to be gained in sensitivity by utilizing perfectly squeezed light; this is equivalent to a very welcome factor-of-50 increase in light power.

The improvement in sensitivity by use of squeezed light is even more limited by imperfect components than the power enhancement due to recycling. Let us again consider the example mentioned at the end of Sec. VIII: the fluctuations in the index of refraction on a scale of decimeters of about 2×10^{-7} in a beam splitter made of fused silica. In a large-scale interferometer the relative interference minimum is then expected to be deteriorated to approximately 1%. According to Eq. (36) the possible improvement in sensitivity by use of squeezed states of light would only be a factor of 2.

IX. CONCLUSION

To reach the ultimate sensitivity of laser interferometers, as planned for the gravitational wave detectors, the light power inside the interferometer has to be extremely high. In a detector with a storage time adapted to millisecond pulses, the $1\,\sigma$ value of the shot noise for 1 kW of light power (as defined in Sec. VII) corresponds to signals at a strain level of 10^{-21}. A further increase of the sensitivity by a factor of 10 implies an increase in light power by a factor of 100. In case Fabry-Pérot cavities are used instead of delay lines to realize the long light path,

the intensity at the reflection spots will be even higher, by roughly twice the number of effective reflections at these mirrors.

A storage time adapted to signals at lower frequencies considerably reduces the power level required for a given strain sensitivity. Very high light powers are likely to degrade the performance of the interferometer because of wave-front deformation as a consequence of the substrates being locally heated by the illuminating light. One mechanism is the surface deformation because of thermal expansion and the second one is thermal lensing in a substrate with a temperature gradient in the region of the passing beam. The temperature gradient may occur due to absorption at the coating or inside the substrate. In this paper both these effects have been treated quantitatively.

The surface deformation scales proportionally to the ratio α/κ between the thermal expansion coefficient and the thermal conductivity, whereas thermal lensing scales with the ratio β/κ between the temperature dependence of the index of refraction and the thermal conductivity. Fused silica seems not to be the best choice, particularly in the case where the beam is transmitted through the substrate. Better would be sapphire, provided it can be produced in the required size and purity; it shows a much smaller value for β/κ. As long as the beam is only reflected and not transmitted, ULE and silicon with their low values of α/κ are possibly the best materials that can realistically be considered for being used as mirror substrates; silicon may be somewhat preferable because of its higher mechanical quality factor. The low mechanical quality factor of Zerodur does not allow this material to be implemented in an interferometric gravitational wave antenna. The optimal material would be diamond because of its unsurpassed combination of thermal and mechanical properties.

The relations derived have demonstrated how extremely critical an asymmetry may be for the performance of a Michelson interferometer. For a delay-line system one can tolerate a fairly high absorption level if all mirrors show the same homogeneous absorption. For a difference of less than 10% in the average absorption between the four mirrors and a statistical fluctuation of also only a few percent, the local mirror deformation in sagitta is allowed to be up to $2\lambda/N$ for the minimum to stay below 10^{-3}. For an asymmetric interferometer with one mirror absorbing significantly more (say, at least by a factor of 1.5) than the other ones, a local mirror deformation as small as $\lambda/(6N)$ is sufficient to produce the same minimum of 10^{-3}.

As far as thermal effects are concerned, one does not gain by using light with longer wavelengths, provided the absorption and $\partial n/\partial T$ are wavelength independent. What counts for the shot-noise-limited performance is the ratio between wavelength and light power. The higher power results in a correspondingly larger wavefront deformation, giving the same deterioration of the interference quality. In practice, the losses, particularly the absorption, are usually less for longer wavelengths. On the other hand, a wavelength larger by a factor m demands a mirror diameter bigger by $\sqrt{m}$, which is very inconvenient for delay-line systems.

The discussions of this paper have been limited to interferometers not using signal recycling, as proposed by Meers [9] (*dual recycling*). It is not yet clear how the implementation of an extra mirror (or perhaps even a mode-cleaner cavity) in front of the photodiode will affect the response of the whole system to thermal effects; there are some indications that the losses due to mode conversion into low-order transverse modes can at least partly be recovered this way. This question goes beyond the intention of this paper and is subject to current investigation.

As has been shown in this paper, the problem of wavefront deformation—particularly the one arising from thermal effects—needs careful attention in interferometers designed for the high level of light power necessary to detect gravitational waves. Fortunately, continuous improvement is going on in the development of high quality coatings and substrate materials. It is hoped that diamond will become available at some time as a substrate material in the required size and purity [25]. In that case even power levels of several 100 kW do not appear unrealistic as far as heating problems are concerned.

ACKNOWLEDGMENTS

We want to thank Tim Niebauer, and also the Glasgow group, particularly Brian Meers, for helpful discussions. This work was supported by the Bundesministerium für Forschung und Technologie (BMFT).

[1] J. Hough *et al.*, Max-Planck-Institut für Quantenoptik Internal Report No. MPQ 147, 1989 (unpublished); available from the authors on request.

[2] Laser Interferometer Gravitational Wave Observatory (LIGO) Report, 1989, Vols. 1 and 2 (unpublished); available from the authors on request.

[3] VIRGO Report, 1987 (unpublished); available from the authors on request.

[4] K. S. Thorne, in *300 Years of Gravitation*, edited by S. W. Hawking and W. Israel (Cambridge University Press, Cambridge, 1987).

[5] K. Maischberger, A. Rüdiger, R. Schilling, L. Schnupp, D. H. Shoemaker, and W. Winkler, Max-Planck-Institut für Quantenoptik Internal Report No. MPQ 96, 1985 (unpublished); revised edition, MPQ 129, 1987 (unpublished).

[6] D. Herriot, H. Kogelnik, and R. Kompfner, Appl. Opt. **3**, 523 (1964).

[7] W. Winkler, in *The Detection of Gravitational Radiation*, edited by D. Blair (Cambridge University Press, Cambridge, 1991).

[8] J. Hough, B. J. Meers, G. P. Newton, N. A. Robertson,

H. Ward, B. F. Schutz, and R. W. P. Drever, University of Glasgow Design Study Report No. GWD/RAL/86–001, 1986 (unpublished).
[9] B. J. Meers, Phys. Rev. D **38**, 2317 (1988).
[10] C. M. Caves, Phys. Rev. D **23**, 1693 (1981).
[11] J. Gea-Banacloche and G. Leuchs, J. Opt. Soc. Am. B **4**, 1667 (1987).
[12] J. Gea-Banacloche and G. Leuchs, J. Mod. Opt. **36**, 1277 (1989).
[13] M. A. Olmstead, N. M. Amer, and S. Kohn, Appl. Phys. A **32**, 141 (1983).
[14] A. C. Boccara, D. Fournier, W. Jackson, and N. M. Amer, Opt. Lett. **5**, 377 (1980).
[15] P. Hello and J. Y. Vinet, J. Phys. (Paris) **51**, 2243 (1990).
[16] R. Weiss, MIT Research Laboratory of Electronics Report No. 105, 1972 (unpublished).
[17] A. Brillet (private communication).
[18] W. Englisch (private communication).
[19] H. Kogelnik, Bell Syst. Tech. J. **44**, 455 (1965).
[20] A. E. Siegmann, *Lasers* (University Science Books, Mill Valley, CA, 1986).
[21] H. Billing, K. Maischberger, A. Rüdiger, R. Schilling, L. Schnupp, and W. Winkler, J. Phys. E **12**, 1043 (1979).
[22] *The Detection of Gravitational Radiation*, edited by D. Blair (Cambridge University Press, Cambridge, 1991).
[23] D. Shoemaker, R. Schilling, L. Schnupp, W. Winkler, K. Maischberger, and A. Rüdiger, Phys. Rev. D **38**, 423 (1988).
[24] M. Xiao, L. A. Wu, and H. J. Kimble, Phys. Rev. Lett. **59**, 278 (1987).
[25] S. Hagstrom (private communication).